Side-Chain Liquid Crystalline Polymer Networks: Exploiting Nanoscale Smectic Polymorphism To Design Shape-Memory Polymers

Suk-kyun Ahn,[†] Prashant Deshmukh,[‡] Manesh Gopinadhan,[§] Chinedum O. Osuji,[§] and Rajeswari M. Kasi[†,‡,*]

[†]Polymer Program, The Institute of Materials Science, and [‡]Department of Chemistry, University of Connecticut, Storrs, Connecticut 06269, United States, and [§]Department of Chemical and Environmental Engineering, Yale University, New Haven, Connecticut 06520, United States

ABSTRACT Herein, we investigate the influence of nanoscale smectic polymorphism within end-on fixed side-chain liquid crystalline polymer networks (SCLCNs) on macroscopic shape-memory and actuation properties. We have synthesized a series of SCLC-type linear (TP-n) and cross-linked random terpolymers (XL-TP-*n*) with varying length of flexible methylene spacers ($n = 5$, 10, and 15) between polynorbornene main-chain and cholesteryl ester side-chains. Thermal and mechanical analyses by differential scanning calorimetry (DSC) and dynamic mechanical analysis (DMA) confirm a glass transition (T_g), a clearing temperature (T_{cl}), and a network structure in the XL-TP-*n*. Detailed structural investigation conducted using wide-angle and small-angle X-ray scattering (WAXS and SAXS) at room temperature proves self-assembled smectic A (SmA) polymorphism of the XL-TP-*n* which evolves from non-interdigitated bilayer (SmA_2) for $n = 5$ to mixed layers of monolayer-like highly interdigitated layer (SmA_1) and SmA_2 for $n = 10$ and to SmA_1 for $n = 15$. In addition, TP10 at temperatures above 60 °C interestingly shows transformation of SmA structure from mixed layer ($SmA_1 + SmA_2$) to interdigitated structure (SmA_d). The SmA polymorphism developed in TP-*n* during shape-memory cycles (SMCs) significantly impacts the ultimate strain responses. A mechanism for the unique interdigitation-based thermostrictive behavior is proposed. More importantly, this new actuation mechanism observed in these XL-TP-*n* can be exploited to develop intelligent thermal actuators.

KEYWORDS: shape-memory materials · liquid crystals · self-assembly · nanostructured smart materials · structure–property relationships · actuators

Shape-memory polymers (SMPs) are a fascinating class of smart polymers which can recover a predefined shape from a temporarily programmed shape by application of external stimulus, typically heat. Research on SMPs has rapidly grown in the past decade because of their potential opportunities in different areas including biomedical materials,[1−4] such as apparatuses for minimally invasive surgery,[5] self-expandable stents,[6,7] tissue engineering scaffolds,[8−10] and controlled drug release vehicles,[11−14] as well as smart multifunctional materials[15] in shape/color changing sensors,[16,17] substrates for lithography[18] or spatially localized surface wrinkles,[19] reversible adhesive systems,[20,21] and textiles.[22]

Thermally induced SMPs, which represent a major and fundamental class of current SMPs, are based on exploiting one or more phase transition temperatures (T_{trans}) such as glass transition (T_g), melting transition (T_m), or liquid crystalline clearing transition (T_{cl}) to trigger shape-memory effect (SME). The SME can be typically divided into two processes called programming and recovery process. The programming process is the procedure to create a desired temporary shape by manipulating external force and temperature of a predefined permanent shape. During this process, the temporary shape can be obtained by deformation of the SMP at the elevated temperature above T_{trans} to gain enough flexibility of the polymeric chain, followed by cooling the SMP under constant stress to below T_{trans} to solidify the deformed shape by physical cross-links such as virtrification or crystallization. In the recovery process, the SMP recovers the permanent shape by reheating the SMP above T_{trans} under stress-free conditions. The entropy elasticity is the driving force to recover the coiled permanent shape from the strained temporary shape.

Liquid crystalline elastomers (LCEs) or liquid crystalline polymer networks (LCNs) have been also considered as interesting candidates for SMPs as well as artificial muscles because the coupling between ordered LC phases and polymeric networks produces a unique thermostrictive property. LCEs have been actively investigated as an alternative for piezoelectrics, hydrogels, conducting polymers, dielectric elastomers, and many other polymer systems for use as artificial muscles or actuators.[23,24] The reversible shape change in the LCEs is mainly enabled by the conformational change of polymer chains between

* Address correspondence to kasi@ims.uconn.edu.

Received for review January 19, 2011 and accepted March 14, 2011.

Published online March 14, 2011
10.1021/nn200211c

elongated anisotropic state (prolate or oblate) and contracted isotropic state (spherical) upon application of heat.[23,25,26] Various types of LCEs and their principle mechanisms for the use in sensors and actuators are well-documented in a recent review article.[23]

LCEs or LCNs have also received increasing attention to develop smart functional polymers including SMPs. Mather and co-workers have developed smectic C (SmC) and nematic (N)-type main-chain liquid crystalline elastomer and network (MCLCE and MCLCN), respectively, that show exceptional SME and actuation behavior.[27,28] Recently, the same group has demonstrated an interesting surface SME by using siloxane-based MCLCE, which can be used as a template for soft lithography.[18] Hiraoka and Finkelmann have reported that molecular tilt during the LC phase change between smectic A (SmA) and chiral SmC (SmC*) can also trigger reversible SME upon heating and cooling.[29,30] Terentjev and co-workers have prepared a shape-memory fiber by MCLC triblock copolymers of which N-type midblock is responsible for reversible actuation, while terphenyl end blocks form a micellar phase-separated morphology for physical networks.[31] The triblock liquid crystalline polymer has been aligned by fiber extrusion and drawing and therefore exhibits remarkable reversible elongation and contraction of about 500% strain. However, we would like to note that the last two examples may also be classified as artificial muscles or thermal actuators rather than just SMPs because typical SMEs are featured by both programming and recovery process with manipulation of both temperature and force.

Recently, our group has also reported a random terpolymer comprising a SmA-type side-chain liquid crystalline polymer network (SCLCN) which has the capability of showing three different SMEs by programming shape-memory cycles (SMCs) with dual transition temperatures (T_g and T_{cl}).[32] In the present publication, a series of SCLC-type linear and cross-linked terpolymers (TP-*n* and XL-TP-*n*) are prepared, which exhibit nanoscale SmA polymorphism at room temperature from a non-interdigitated bilayer (SmA_2) for $n = 5$ to mixed layers containing SmA_2 and monolayer-like highly interdigitated layer (SmA_1) for $n = 10$ and to SmA_1 layer for $n = 15$. Additionally, TP10 at temperatures above 60 °C exhibits transformation of SmA structure from mixed layer ($SmA_1 + SmA_2$) to interdigitated structure (SmA_d). Depending on the SmA polymorphism, the strain response is dramatically altered during the programmed SMCs. Moreover, we demonstrate that the microstructure evolution of the SmA phase at the nanoscale, which originates from different extents of interdigitation of side-chain cholesteryl mesogen, actually determines the strain response (elongation and contraction) during SMCs. To the best of our knowledge, this interdigitation-based thermostrictive property has not been observed before. We believe our novel end-on fixed SCLCNs can provide a new mechanism to develop thermal actuators.

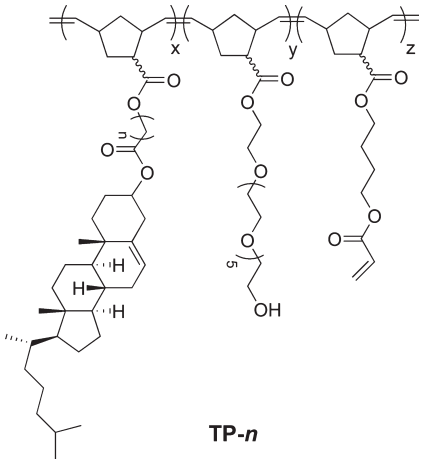

Figure 1. Chemical structure of SCLC-type random terpolymers (TP-*n*), where *n* = 5, 10, and 15.

RESULTS AND DISCUSSION

Preparation of SCLC-Type Terpolymers (TP-*n*). A series of end-on fixed SCLC-type random terpolymers (TP-*n*, Figure 1) are prepared by ring-opening metathesis polymerization (ROMP) of three different monomers using Grubbs catalyst second generation. The three different monomers 5-{*n*-(cholesteryloxycarbonyl)-alkyloxycarbonyl}bicyclo[2.2.1]hept-2-ene (NBCh-*n*), poly(ethylene glycol)-functionalized norbornene (NBPEG), and 5-(acryloyl butoxycarbonyl)bicyclo[2.2.1] hept-2-ene (NBBA) are synthesized according to the procedures described in our previous publication.[32,33] Each monomer has a unique function in the TP-*n*, where (1) NBCh-*n* provides LC ordering, (2) NBPEG helps to tailor thermal and mechanical properties such as transition temperature (T_g and T_{cl}) or toughness, and

TABLE 1. Synthesis of SCLC-Type Terpolymers (TP-*n*)

	mol %[a]					
polymer	NBCh-*n*	NBPEG	NBBA	yield (%)	M_n (kg/mol)[b]	PDI[b]
TP5	81.8	15.8	2.4	89.5	145	1.60
TP10	82.3	15.2	2.5	91.4	75	1.92
TP15	80.5	15.5	4.0	89.4	97	1.54

[a] Calculated from ^{1}H NMR. [b] Obtained from GPC with THF as eluent and calibrated with PS standards.

TABLE 2. Thermal Properties of Linear and Cross-Linked Terpolymers (TP-*n* and XL-TP-*n*) Determined by DSC

polymer	*G* (%)[a]	T_g (°C)	$T_{LC\text{-}LC}$ (°C)	ΔH for $T_{LC\text{-}LC}$ (J/g)	T_d (°C)	ΔH for T_d (J/g)
TP5		29.7			94.5	3.3
XL-TP5	91.0	32.1			94.0	2.7
TP10		25.4	61.6	0.7	94.2	2.4
XL-TP10	82.0	28.6	61.8	0.8	93.3	2.5
TP15		23.0			104.1	5.5
XL-TP15	89.0	22.5			103.5	5.4

[a] *G*: gel fraction determined from mass ratio between before and after Soxhlet extraction by THF as solvent.

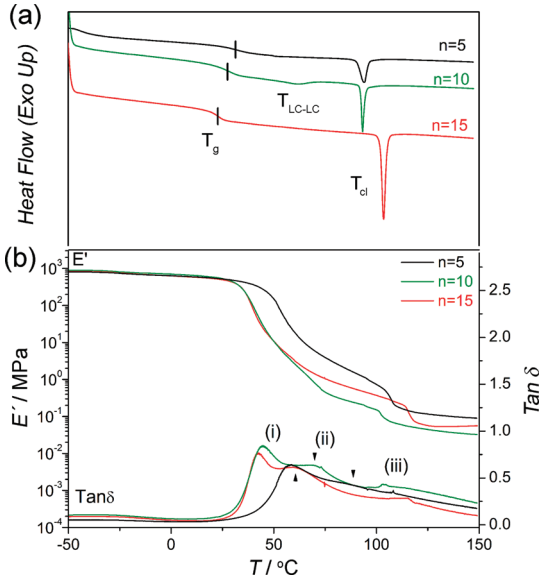

Figure 2. Thermal and linear viscoelastic properties of XL-TP-*n* (black for XL-TP5, green for XL-TP10, and red for XL-TP15): (a) first heating DSC thermogram of XL-TP-*n* with a heating rate of 10 °C/min and (b) tensile storage modulus (E') and tan δ trace measured by DMA. Tan δ reveals three characteristic relaxation peaks for each XL-TP-*n*, where peaks (i) for T_g, peaks (ii) for polydomain−monodomain transition, and peaks (iii) for T_{cl}.

(3) NBBA affords potential cross-linkable sites by either heat or light. More importantly, the length of flexible methylene spacer between polynorbornene main-chain and cholesteryl side-chains can be varied ($n = 5$, 10, and 15), which essentially induces diversified microstructures within LC order.

Table 1 summarizes molecular characterization data of TP-*n* determined by using ^{1}H NMR and gel permeation chromatography (GPC). The TP-*n* contains more than 80 mol % of monomer containing cholesteryl mesogen (NBCh-*n*), about 15 mol % of short-chain PEG monomer (NBPEG) as an internal plasticizer, and less than 4 mol % of cross-linkable monomer (NBBA). As a result, the final structure and property of resulting TP-*n* is expected to be governed by NBCh-*n*. In all cases, TP-*n* of approximately 100 kDa molecular weight with respect to the polystyrene (PS) standards is obtained with moderate polydispersity.

Thermal and Linear Viscoelastic Properties. The presence of network structure is one of the key requirements for SMPs because it prevents the polymeric chain from slipping off each other and also determines the permanent shape during the curing process. Therefore, we synthesized cross-linked terpolymers (XL-TP-*n*) from the linear terpolymers (TP-*n*) by thermally curing the acrylate end group in the NBBA in the absence of thermal initiators. A film of the TP-*n* is first prepared by compression molding of the sample at 20−30 °C above T_g. Subsequently, the compressed film is placed inside a vacuum oven and cured at 120 °C ($>T_{cl}$) for 48 h between two hot plates, resulting in a cross-linked film with uniform thickness. Gel fraction (*G*) values determined from the ratio between mass before and after Soxhlet extraction with THF are reasonably high (82−91%) for XL-TP-*n*. Incomplete cross-linking ($G <$ 100%) is probably due to the restricted mobility of acrylate groups during the melt-state curing process. Nevertheless, the presence of un-cross-linked chains will not significantly influence or alter the final property of the SCLCNs.[23]

Thermal transitions and associated enthalpies (ΔH) of TP-*n* and XL-TP-*n* are determined by a second heating cycle of differential scanning calorimetry (DSC), and these values are listed in Table 2. The transition temperature (T_g and T_{cl}) and ΔH of T_{cl} are only slightly different before and after curing due to the formation of lightly cross-linked networks when cured in the absence of thermal initiators. This also implies that the fundamental mesomorphic structure of TP-*n* is not significantly altered by the curing process.

Figure 2 compares the first heating cycles of DSC and dynamic mechanical analysis (DMA) for XL-TP-*n* with a ramp rate of 10 and 3 °C/min, respectively. From Figure 2a and Table 2, it is observed that XL-TP-*n* displays well-separated T_g and T_{cl}; however, XL-TP10 exhibits an additional broad transition between T_g and T_{cl}. The extra phase transition is attributed to a LC-LC phase transition ($T_{LC\text{-}LC}$) as determined by temperature-controlled small-angle X-ray scattering (SAXS), which will be discussed in greater detail in the next section. DMA is employed to confirm the network structure of XL-TP-*n* and to investigate their relaxation behaviors, which cannot be determined from DSC alone. As observed in DSC, two well-separated transitions corresponding to T_g and T_{cl} are also clearly detected in DMA during heating, which are reflected

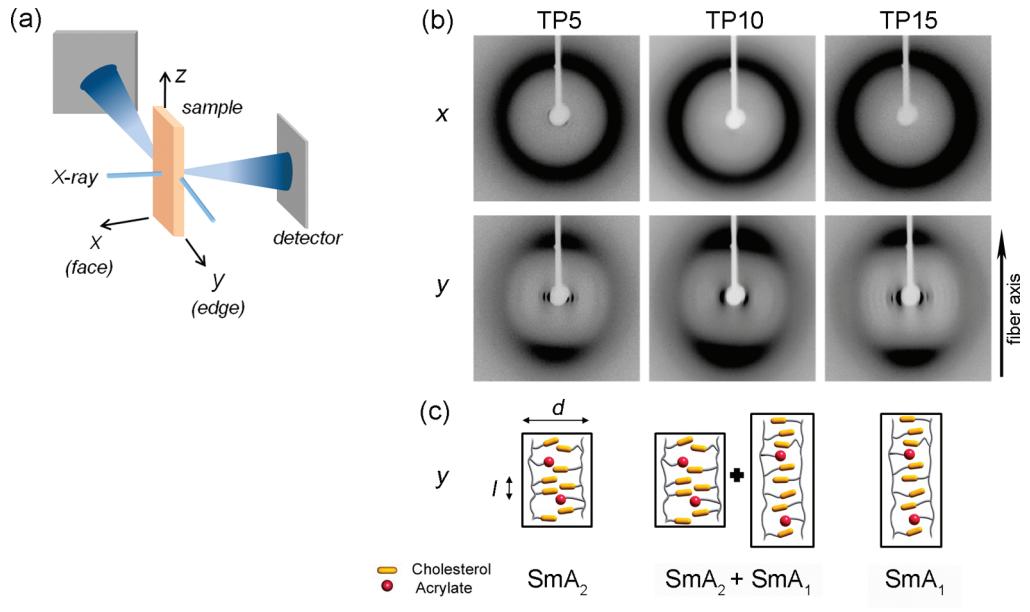

Figure 3. WAXS experiment at room temperature for TP-*n*: (a) geometry of experimental setup in the 2D WAXS experiment, (b) 2D WAXS patterns in which X-ray beam is directed along the normal (*x*-direction) and lateral (*y*-direction) to the film, and (c) illustration of molecular packing structure of TP-*n* in the *y*-direction, where *d* represents the thickness of SmA layer and *l* represents the lateral spacing of cholesteryl mesogens.

as reduction in storage modulus (E') and characteristic relaxation peaks in the tan δ trace, denoted as (i) for T_g and (iii) for T_{cl}. As the temperature is further increased beyond T_{cl}, E' reaches a rubbery plateau, indicating successful formation of network structures within XL-TP-*n*. The T_{LC-LC} of XL-TP10 observed at 61.8 °C in the DSC thermogram is not clearly detected by change in either E' or the tan δ peak in DMA. Lastly, additional peaks (ii) in the tan δ trace are detected between T_g and T_{cl} of XL-TP-*n* as indicated by three arrows. We speculate that these peaks might be because of (1) dynamic soft elasticity[28] and/or (2) relaxation from LC order.[34,35] The first premise originates from energy dissipation during polydomain to monodomain transition upon loading, which results in the reorientation of LC domain. The second hypothesis is attributed to the large decoupling motion between the polynorbornene main-chain and cholesteryl side-chains. In other words, sufficient length of methylene spacer in NBCh-*n* distinctly separates movement of cholesteryl side-chains from the main-chain so that the relaxation of ordered cholesteryl mesogens can be independently observed from the tan δ trace beyond relaxation of T_g of the polynorbornene main-chain. This might result in relatively sharp peaks and stronger intensity in tan δ for the longer methylene spacer (XL-TP10 and XL-TP15), while a weak and broad shoulder is found in the short methylene spacer (XL-TP5). To comprehensively understand the relaxation behavior of XL-TP-*n*, further rheological study of these polymers will be necessary,[36] which is beyond the scope of the present paper. Nevertheless, we surmise that the difference in tan δ is possibly because of the varied microstructures at the molecular level in XL-TP-*n*, and this will be discussed in the next section.

Microstructural Analysis. To investigate detailed LC morphology of TP-*n*, both wide-angle and small-angle X-ray scattering (WAXS and SAXS) are employed. Figure 3 shows 2D WAXS of TP-*n* recorded at room temperature with films prepared by compression molding at 20−30 °C higher than T_g at which no cross-linking reaction occurs. In the 2D WAXS, the films of TP-*n* show strong anisotropy in the scattering pattern depending on the exposure direction of the X-ray beam. When the edge of films is positioned normal to the X-ray beam (*y*-direction), characteristic SmA scattering patterns and orientations are observed. In contrast, only isotropic scatterings are detected if the face of the films is exposed to X-ray beam (*x*-direction). The anisotropic scattering patterns of TP-*n* suggest that the ordering of cholesteryl mesogens is confined only in the edge of the film (*y*-direction) due to the generation of squeezing flow in the radial direction while compressing the samples to the *x*-direction (Figure S1 in Supporting Information). Lastly, WAXS study shows that scattering patterns on the equator represent the thickness (*d*) of smectic layers and broad halo on the meridian represents lateral spacing (*l*) of cholesteryl mesogens in TP-*n* (Figure 3c).

Table 3 summarizes *d* spacing values of TP-*n* obtained from X-ray analyses. The cholesteryl side-chain length of TP-*n* is calculated by Materials Studio 4.4 assuming a fully extended structure to determine the microstructure of SmA mesophase by comparing the calculated length of side-chains with experimentally obtained layer spacing. Here, we would like to note

that the *d* spacing values of TP-*n* and XL-TP-*n* do not show significant difference due to the lightly cross-linked nature of XL-TP-*n*. Therefore, fundamentally, the same mesomorphic structure is expected in TP-*n* and XL-TP-*n*. The cholesteryl side-chain of TP-*n* is mainly responsible for the thickness of the SmA layer because it is not only a rigid moiety but also the major constituent of TP-*n* (>80 mol %). In fact, the SmA layer of TP-*n* expands when compared to their homopolymer analogues.[37] The expansion of the SmA layer is attributed to the dilution effect[38−40] of mesogenic monomer (NBCh-*n*) by the incorporation of two other nonmesogenic monomers (NBPEG and NBBA). The introduction of nonmesogenic monomers leads to swelling of a main-chain-rich sublayer within the entire microphase-separated SmA layer which comprises both main-chain-rich and mesogen-rich sublayers.[38,39]

Smectic-based end-on fixed side-chain liquid crystalline polymers (SCLCPs) can display unique hierarchical self-assembled morphologies within smectic layers that result from the interdigitation of side-chain mesogens in the preferred antiparallel direction.[41] This interdigitation of side-chain mesogens is generally induced by two different mechanisms depending on the types of mesogens.[42] When mesogens have a polar terminal group such as cyano (−CN) or nitro ($-NO_2$), the dipolar interaction of mesogens between polymer interchains can induce interdigitated smectic layers.[42−44]

TABLE 3. Layer Spacing of TP-*n* Determined from X-ray Scattering at Room Temperature

polymer	d_1 (Å)	d_2	d_3	side-chain length (Å)[a]
TP5	59.6	29.9	20.9	28.4
TP10	73.9	40.6	24.6	35.3
TP15	47.9	24.3	16.3	42.7

[a] Calculated value of cholesteryl side-chain assuming a fully extended structure.

Interdigitated smectic layers are also preferred in mesogens possessing strong asymmetry in the molecular shape due to steric interactions.[42] The latter is also found in our TP-*n* where the steric interaction between cholesteryl ester side-chains is enhanced with increasing length of methylene spacer (*n* = 5, 10, and 15).

For TP5 and TP15, the ratio between d_1, d_2, and d_3 is approximately 1:1/2:1/3, which indicates d_2 and d_3 are second and third order of d_1, respectively. The calculated cholesteryl side-chain length of TP5 is nearly half the value of d_1, and thereby SmA_2 is proposed for TP5. The side-chain length of TP15, whose motion of cholesteryl side-chains is the most decoupled from the polymer backbone by the 15 methylene spacer, is comparable to d_1 such that SmA_1 is predicted. For TP10, there is no correlation between d_1 and d_2, implying that more than a single type of smectic layer is present in this system.[45−47] The cholesteryl side-chain length of TP10 is close to half of d_1, suggesting SmA_2 while d_3 is attributed to the third-order reflection of d_1. In addition, slightly higher value of d_2 compared to the cholesteryl side-chain is most likely ascribed to the SmA_1 structure. Schematic cartoons in Figure 3c show the possible mesomorphic structures of TP-*n* as described above. To summarize, increasing the length of the flexible methylene spacer in TP-*n* induces a higher extent of interdigitation of cholesteryl side chains, resulting in rich SmA polymorphism in the nanometer scale.

In previous DSC analyses (Table 2 and Figure 2), TP10 exhibits a unique broad phase transition designated as $T_{LC\text{-}LC}$, while TP5 and TP15 do not show any LC-LC transition. Further analysis is performed on TP10 to identify the transition by temperature-controlled SAXS (Figure 4a,b). Initially, three reflection peaks, whose *d* spacing values correspond to 73.9, 40.6, and 24.6 Å, reflecting for mixed layer (SmA_1 + SmA_2) are

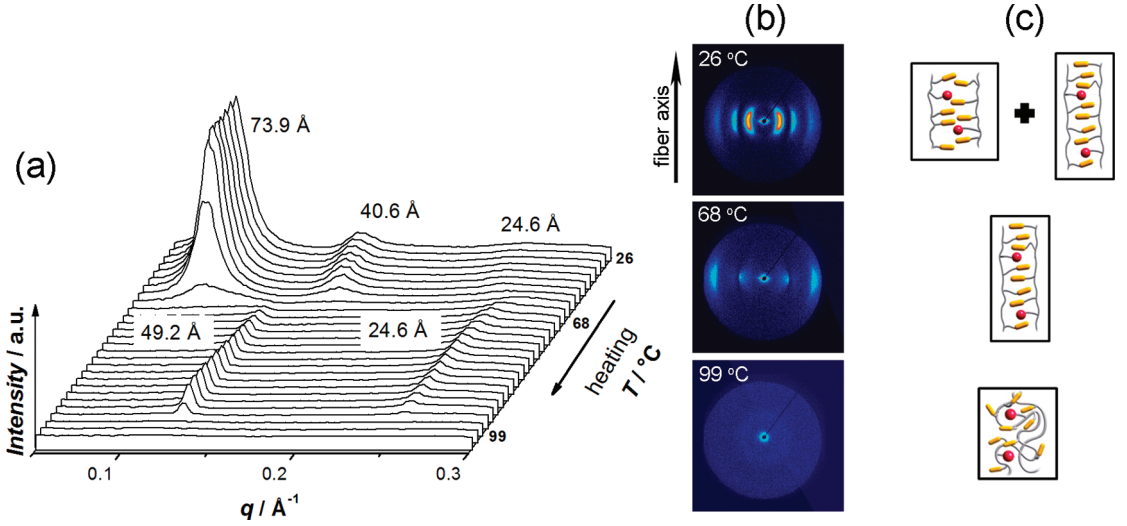

Figure 4. Temperature-controlled SAXS analysis of TP10: (a) SAXS profile during heating scan, (b) 2D SAXS images during heating, and (c) evolution of SmA layer during heating.

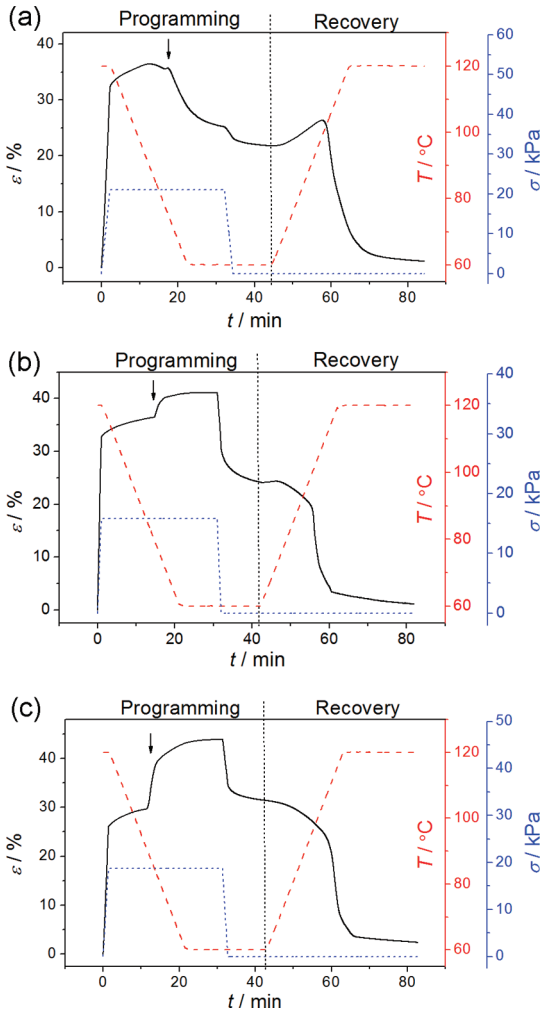

Figure 5. Strain responses of XL-TP-*n* during T_{cl}-based one-way shape-memory cycle (1W-SMC, fourth cycle): (a) XL-TP5, (b) XL-TP10, and (c) XL-TP15. Temperature range (60−120 °C) only includes T_{cl} of XL-TP-*n*.

observed at room temperature. Interestingly, these peaks are clearly shifted to a larger angle at temperature ranges from 60 to 70 °C, which agrees well with $T_{LC\text{-}LC}$ from DSC result. Moreover, when comparing the experimentally determined shifted *d* spacing values of 49.2 and 24.6 Å at higher temperature with calculated side-chain length, it is expected that SmA_d-type lamellar morphology is predominant at a temperature above $T_{LC\text{-}LC}$. Therefore, the SAXS results indicate that the $T_{LC\text{-}LC}$ is a transition where the initial mixed layers (SmA_1 + SmA_2) at room temperature evolve to the SmA_d layers upon heating, as illustrated in Figure 4c. Both SAXS and WAXS preserve the same scattering patterns (small-angle reflection peaks on the equator and wide-angle amorphous halo on the meridian) at temperatures below and above $T_{LC\text{-}LC}$ and finally disappear at 99 °C (Figure 4b and Figure S2 in Supporting Information).

Shape-Memory Properties. We have explored shape-memory properties of XL-TP-*n* by means of cyclic

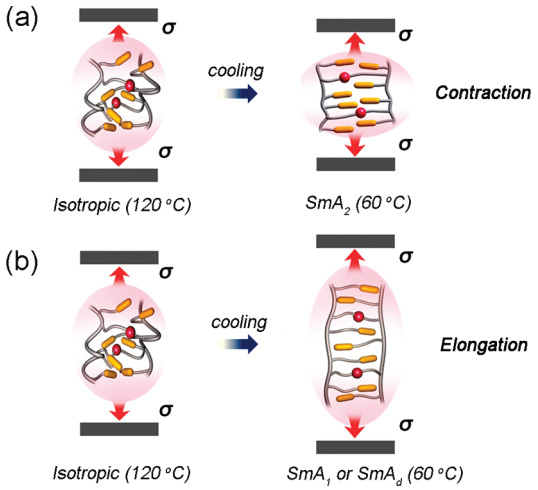

Figure 6. Schematic illustration of the mechanism of elongation and contraction for XL-TP-*n* when cooling from isotropic to SmA mesophase under constant stress: (a) formation of SmA_2 induces macroscopic contraction of the sample for XL-TP5, and (b) formation of SmA_d or SmA_1 results in macroscopic elongation of the sample for XL-TP10 and XL-TP15, respectively. SmA_d and SmA_1 are not distinguished in panel b, and elongation is not drawn to scale.

thermomechanical analysis using DMA. Covalent networks are introduced to avoid de-entangling of polymers and to improve shape recovery.[32] Previously, we have shown that both T_g and T_{cl} can serve as T_{trans} to trigger SME.[32] In the present paper, we are particularly interested in exploring the influence of spacers in XL-TP-*n*, which allows for SmA polymorphism in the nanometer scale, on macroscopic shape-memory properties of these materials. Therefore, two independent SMCs are created by using T_{cl} as T_{trans}, which triggers SME. The first SMC is the one-way shape-memory cycle (1W-SMC)[48,49] where each cycle consists of four consecutive steps: (1) deformation above T_{trans}, (2) cooling below T_{trans} under constant stress, (3) unloading, and (4) recovery by reheating above T_{trans}. The second SMC simply involves continuous heating and cooling across T_{trans} under constant stress, referred to as the two-way SMC (2W-SMC).[28,48,50] Four successive SMCs are performed for both 1W- and 2W-SMC. Detailed procedures can be found in the Experimental Section. We would like to note that the applied stress (5.0−21.0 kPa) during 1W- and 2W-SMCs is rather low because of the low storage moduli of XL-TP-*n* at the rubbery plateau region.

Shape-memory properties are typically characterized by shape fixity ratio (R_f) and shape-recovery ratio (R_r) that can be obtained through the analysis of SMCs. R_f represents the ability of the material to preserve a temporarily fixed strain after unloading, and R_r describes the ability of the material to restore an original strain after completion of recovery. We evaluate R_f and R_r of the T_{cl}-based 1W-SMCs by using following

equations[51,52]

$$R_f(\%) = \frac{\varepsilon_u(N) - \varepsilon_p(N-1)}{\varepsilon_l(N) - \varepsilon_p(N-1)} \times 100$$

$$R_r(\%) = \frac{\varepsilon_u(N) - \varepsilon_p(N)}{\varepsilon_u(N) - \varepsilon_p(N-1)} \times 100$$

where ε_u is the strain after unloading, ε_l is the strain with load before unloading, ε_p is the strain after recovery, and N is the number of cycles. In the following paragraphs, we will present shape-memory behaviors of XL-TP-*n* during T_{cl}-based 1W-SMCs, the potential mechanism for the different strain responses, quantitative analyses of 1W-SMCs, and finally 2W-SMCs.

Figure 5 shows the strain responses of XL-TP-*n* as a function of temperature and stress during the fourth cycle of T_{cl}-based 1W-SMC. For comparison purposes, relatively similar initial strain (25−32%) is applied to all XL-TP-*n*. In all cases, the strain of XL-TP-*n* is initially increased by application of stress at an isotropic state (120 °C) and finally recovered at T_{cl} according to the programmed 1W-SMCs (steps 1−4). However, remarkable difference in the strain responses among XL-TP-*n* is observed when the sample is cooled from 120 to 60 °C under constant stress as indicated by arrows. During this cooling process, the strain decreases for XL-TP5, while both XL-TP10 and XL-TP15 exhibit strain increase. This is because XL-TP-*n* develops different types of SmA microstructure when cooled from an isotropic state, which leads to either macroscopic contraction or elongation. In principle, the director of SmA layers develops perpendicular to the polymer main-chain guided by an applied stress field in the loading direction due to end-on fixed SCLCP architecture. Then, the collective growth of SmA layers results in macroscopic dimensional change of the XL-TP-*n*.

The varied strain responses of XL-TP-*n* during the cooling process of T_{cl}-based 1W-SMCs can be understood as a result from the formation of nanoscale SmA polymorphism. As discussed in section 2.3, the formation of the SmA_2 layer, mixed layer ($SmA_1 + SmA_2$), and SmA_1 is determined for TP5, TP10, and TP15, respectively, under ambient condition. The TP5 and TP15 preserve nearly the same SmA microstructure before the temperature reaches the isotropic state (Figure S3 in Supporting Information). In contrast, further analysis of TP10 by temperature-controlled SAXS and WAXS proves that the mixed SmA layers ($SmA_1 + SmA_2$) formed at room temperature transform to a SmA_d layer above 60 °C. Consequently, when cooled from 120 °C (isotropic phase) to 60 °C (SmA mesophase) in the T_{cl}-based SMC, XL-TP5 develops an SmA_2 layer, while XL-TP10 and XL-TP15 form SmA_d and SmA_1 layers, respectively.

Figure 6 illustrates that the development of SmA polymorphism of XL-TP-*n* under constant stress essentially determines contraction or elongation of the strain. When SmA layers develop from the isotropic phase, which is assumed to be a spherical configuration, the director of SmA layers is expected to orient perpendicular to the main-chain due to end-on fixed SCLCP architecture. In other words, the developed SmA layer parallel to the applied stress field ultimately leads to the expansion in width compared to the sample width in the isotropic phase. Provided that the density change of the sample is minimal, the sample undergoes contraction in length under constant stress. Moreover, modulus of the sample is increased by the cooling process. Therefore, the

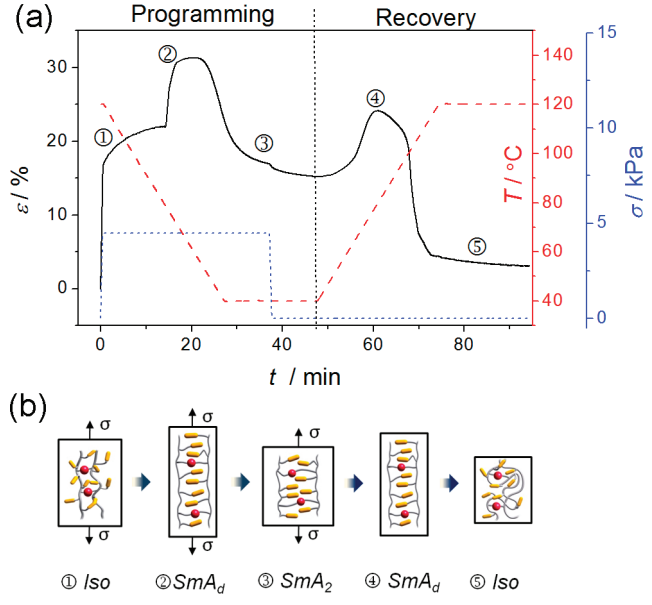

Figure 7. Influence of SmA evolution of XL-TP10 on shape-memory properties: (a) strain responses during T_{cl}-based one-way shape-memory cycle (1W-SMC, fourth cycle) of which temperature range (40−120 °C) includes both T_{LC-LC} and T_{cl}, and (b) corresponding SmA polymorphism change during SMC.

sample length is expected to decrease under constant stress. XL-TP5 follows this predicted strain response, and strain decreases while cooling to 60 °C. In contrast, XL-TP10 and XL-TP15 display increase of strain under similar experimental conditions. The unexpected strain increase is attributed to the formation of SmA_d or SmA_1 layers of XL-TP10 and XL-TP15, respectively. In other words, stacks of cholesteryl side-chains that overlap and order in an interdigitated fashion can overcome the propensity of the SmA layer to expand in width. Therefore, the net elongation is higher in the length direction so that the overall strain of the sample increases during the cooling process. The unexpected strain increase for XL-TP10 and XL-TP15 may also depend on the degree of interdigitation, which is influenced by the methylene spacer length.

To prove the strain variation based on SmA polymorphism, we perform an additional SMC experiment (40—120 °C) using XL-TP10. As demonstrated in temperature-controlled SAXS experiment (Figure 4), XL-TP10 displays the evolution of SmA layers from a mixed layer ($SmA_1 + SmA_2$) to the SmA_d layer across T_{LC-LC}. Therefore, this experiment allows us to investigate the influence of SmA layer transformation on the resulting strain response (Figure 7). When XL-TP10 is cooled to 60 °C under constant stress from an isotropic phase, the strain initially increases as the SmA_d phase is first attained. However, upon further cooling to 40 °C, the strain decreases due to the formation of mixed SmA_2 and SmA_1 layers, where the SmA_2 layer is dominant over the SmA_1 layer as seen from the higher intensity of d_1 than d_2 in the SAXS analysis (Figure 4). In the recovery process, by reheating the sample at a stress-free condition, the strain increases until 80 °C due to the re-formation of the SmA_d layer and thereafter exhibits a sharp recovery at T_{cl}. Accordingly, the evolution of SmA layers at the nanometer scale upon heating and cooling results in significant change in the macroscopic strain response of XL-TP10 during SMC.

The quantitative analyses including strain, R_f, and R_r on the T_{cl}-based 1W-SMCs are listed in Table 4. When the same temperature ranges (60—120 °C) are employed, XL-TP5 had the strongest shape fixation capability (R_f > 91%) compared to XL-TP10 and XL-TP15. This is mainly because the storage modulus of XL-TP5 at 60 °C, where the unloading step is performed, is higher than those of XL-TP10 and XL-TP15 as described in the DMA results in Figure 2. When the temperature for unloading is further decreased to 40 °C, the fixation of the temporary shape is improved for XL-TP10 (R_f > 97%). In general, XL-TP-*n* displays good shape recovering capability. Lastly, we observe continuous strain ($\varepsilon_l(N) - \varepsilon_p(N-1)$) decrease in the 1W-SMCs for XL-TP10 whose temperature range (40—120 °C) includes both T_{LC-LC} and T_{cl} (Figure S4). This is probably because higher orientation in the SmA layer is achieved at higher cycle number, which leads to more distinct strain variation during the phase change between SmA_d and SmA_2.

TABLE 4. Quantitative Analyses of T_{cl}-Based 1W-SMCs for XL-TP-*n*[a]

polymer	strain (%)	R_f (%)	R_r (%)
XL-TP5[b]	26.5	91.7	94.5
XL-TP10[b]	41.3	74.1	96.2
XL-TP15[b]	48.7	79.3	91.4
XL-TP10[c]	19.8[d]	97.7	84.7

[a] Strain: average $\varepsilon_l(N) - \varepsilon_p(N-1)$ for second to fourth cycle; R_f, average shape fixity for second to fourth cycle; R_r, average shape recovery for second to fourth cycle. [b] Temperature range includes 60—120 °C. [c] Temperature range includes 40—120 °C. [d] Strain continuously decreases with increase of cycle number (23.0% for second, 19.6% for third, and 17.0% for fourth cycle).

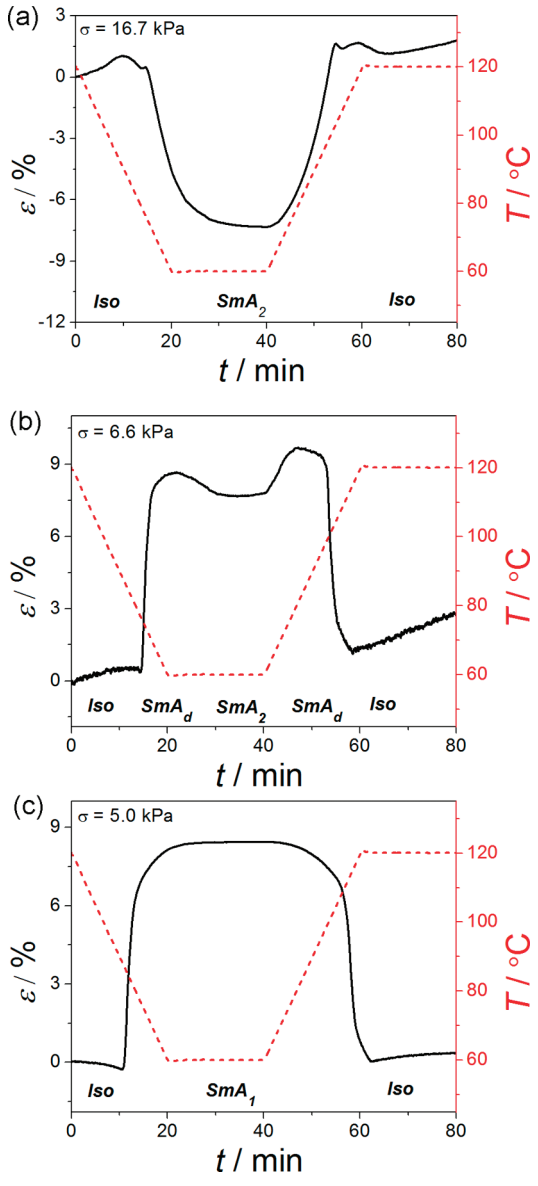

Figure 8. Two-way shape-memory cycles (2W-SMCs, fourth cycle) for XL-TP-*n*: (a) XL-TP5, (b) XL-TP10, and (c) XL-TP15.

We wish to exploit the SmA polymorphism observed in the XL-TP-*n* toward creation of thermal actuators. Therefore, we explored the actuation capability of

XL-TP-*n* by programming 2W-SMCs. Figure 8 shows strain responses of XL-TP-*n* during cooling and heating with a rate of 3 °C/min under constant stress. When the sample is cooled from 120 (isotropic) to 60 °C (SmA mesophase), XL-TP5 contracts due to the formation of a SmA_2 mesophase and expands while heating back to 120 °C. In contrast, the opposite strain responses (expansion when cooling below T_{cl} and contraction when heating above T_{cl}) are observed in XL-TP15, which results from the phase transition between the SmA_1 mesophase and isotropic phase. Lastly, XL-TP10, which contains mixed SmA mesophases, displays either elongation or contraction depending on the temperature window. The 2W-SMC results clearly suggest that the resulting strains of XL-TP-*n* are determined by the development of SmA polymorphsim upon temperature variation. Thus, XL-TP10 and XL-TP15 display a moderate reversible actuation capability (ε = ~8%). To the best of our knowledge, these unique thermostrictive properties based on SmA polymorphism have not been reported before. Therefore, careful selection of the methylene spacer length in the NBCh-*n* will allow for creation of a new class of thermal actuator using our end-on fixed SCLC-type terpolymer.

CONCLUSIONS

We have synthesized a series of end-on fixed SCLC-type linear and cross-linked random terpolymers (TP-*n* and XL-TP-*n*, respectively), where polynorbornene main-chain comprises three different side-chains (cholesteryl mesogen, PEG, and butyl acrylate). These TP-*n* exhibit diversified SmA polymorphism at the nanoscale due to the presence of different length of methylene spacers (n = 5, 10, and 15), which decouples the motion of main-chain polynorbornene from the side-chain cholesteryl mesogen. The covalent networks are introduced in TP-*n* for shape-memory properties by thermal curing, while the fundamental mesomorphic structure of TP-*n* is preserved due to the lightly cross-linked nature of XL-TP-*n*. Thus, direct correlation of X-ray studies performed on TP-*n* with SME performed using XL-TP-*n* is possible. Shape-memory properties of the XL-TP-*n* are strongly influenced by the types of self-assembled SmA mesophases that develop from the isotropic phase. Equally importantly, the evolution of the SmA phase upon temperature change observed in XL-TP10 causes significant change in the shape variation during SMCs. In principle, the director of SmA layers perpendicular to the polymer main-chain allows the resulting strain to decrease in length by expanding in width (XL-TP5). However, we observe the opposite strain responses in XL-TP10 and XL-TP15, which develop the unique interdigitated structure of the SmA phase due to the overlap of rigid cholesteryl side-chain. These interdigitated mesophases show a net increase in strain of the sample in the direction of the applied stress. This is attributed to the dominance of sample elongation (in length) over the propensity of SmA layer expansion (in width) under constant stress when the density change of the sample is minimal. Understanding this influence of microstructural changes on SME will broaden the fundamental knowledge of smart polymeric systems and allows one to exploit this property to develop new types of microactuators.

EXPERIMENTAL SECTION

Synthesis of Terpolymers (TP-*n*). The detailed synthesis procedure and characterization of three monomers (NBCh-*n*, NBPEG, and NBBA) and polymerization of the monomers by ROMP mechanism are reported in our previous publications.[32,33]

Molecular Characterization of Terpolymers. ^{1}H NMR spectra (Bruker DMX 500 MHz NMR spectrometer) are recorded with tetramethylsilane (TMS) as an internal standard and deuterated chloroform ($CDCl_3$) as lock solvent. The monomer composition in synthesized TP-*n* is calculated by comparing the integration ratio of characteristic NMR peaks which correspond to each monomer: 4.6, 3.6, and 5.8 ppm are used to quantify the composition of NBCh-*n*, NBPEG, and NBBA, respectively. Molecular weight and polydispersity indices (PDI) are determined by GPC using a Waters 1515 coupled with a PL-ELS1000 evaporative light scattering (ELS) detector and a Waters 2487 dual wavelength absorbance detector with THF as eluent and polystyrene as standards.

Preparation of Terpolymer Networks (XL-TP-*n*) and Gel Fraction (*G*) Analyses. The linear terpolymers (TP-*n*) in powder form are processed into films with uniform thickness by compression molding at 20−30 °C above their T_g under air. Afterward, the films placed between two hot plates are thermally cured inside a vacuum oven at 120 °C for 48 h. The cured TP-*n* (XL-TP-*n*) are extracted using THF over 24 h to remove un-cross-linked TP-*n*. Gel fraction values (G) of XL-TP-*n* are estimated by the ratio between initial mass before extraction (m_i) and dried mass after extraction (m_d)

$$G(\%) = \frac{m_d}{m_i} \times 100$$

Wide-Angle X-ray Scattering (WAXS) at Room Temperature (Performed at University of Connecticut). WAXS is performed on Oxford Diffraction XCalibur PX Ultra (transmission mode) with Onyx detector (Cu Kα radiation 1.542 Å, double mirror focusing, 40 kV and 40 mA). The specimen for WAXS is prepared by compression molding the powdered sample at about 60 °C, which results in a form of film with uniform thickness. Typical dimension of the specimen for WAXS is 10.0 mm length × 2.0 mm width × 0.7 mm thickness.

Temperature-Controlled X-ray Scattering (Performed at Yale University). SAXS is performed on a pinhole collimated Rigaku instrument (SMAX3000) configured with Cu Kα radiation (1.542 Å) of 1 mm beam diameter produced by a microfocus source. The scattered intensity is registered on a gas-wire electronic area (2D) detector with a resolution of 1024 × 1024 pixels located at a distance of 75 cm from the sample, permitting access to a range of scattering vectors from 0.02 to 0.3 $Å^{-1}$. SAXS patterns are calibrated using silver behenate standard with d spacing of 58.38 Å. One-dimensional integration of the scattered intensity against scattering vector q, where $q = (4\pi/\lambda) \times \sin\theta$, with 2θ the scattering angle, is rendered using MATLAB routines (Rigaku). WAXS is performed onto image plates (Fuji) and calibrated

using Si powder calibration standard with *d* spacing of 3.134 Å. Temperature-dependent measurements are conducted using a hot stage (Linkam THMS600) with an associated temperature controller (TMS 94). For temperature scans, the samples are sandwiched between two thin kapton sheets and the chamber is evacuated and subsequently refilled with helium to provide a low scattering atmosphere that aids heat transfer between the hot stage and the polymer films. Sample temperatures are calibrated using direct read-out from a thermocouple (Omega) attached to the aluminum disk holding the polymer samples. Samples are subjected to a heating/cooling rate of 5 °C/min and allowed to equilibrate for 10 min at each temperature prior to data acquisition.

DSC and DMA Analyses. Thermal properties of TP-*n* and XL-TP-*n* are obtained from DSC (Q100, TA Instruments) under a nitrogen purge. Samples (typical mass of 3−6 mg) are preheated to 150 °C to remove thermal history, and second heating cycles are used to determine T_g, T_{cl}, and ΔH using Universal Analysis software. Thermomechanical properties of XL-TP-*n* are characterized by DMA 2980 (TA Instruments) with cryo accessories attached. Using a tension film mode, preload force of 0.01 N, a heating rate of 3 °C/min, force track (ratio of static to dynamic force) of 125%, and an oscillation frequency of 1 Hz are selected. The amplitude is adjusted during the temperature sweep experiment to provide enough dynamic force at a temperature above T_{cl}. Typical sample dimension for DMA is 6.0 mm (length) × 5.0 mm (width) × 0.5 mm (thickness).

Shape-Memory Characterization. Cyclic thermomechanical analyses are performed on a DMA 2980 apparatus operated in controlled force mode. Two types of SMCs (1W- and 2W-SMCs) are developed using T_{cl} for triggering SME.

For 1W-SMCs, the temperature range includes either 60−120 °C for XL-TP-*n* or 40−120 °C for XL-TP10. Prior to the start of SMC, samples are thermally equilibrated at 120 °C for 30 min. Using XL-TP5 as an example, each 1W-SMC consists of four consecutive steps. These steps include (1) heating the sample to 120 °C and stretching it by ramping force from preload 0.01 to 0.12 N at a rate of 0.05 N/min (deformation), (2) cooling the sample at the rate of 3 °C/min to 60 °C under constant force and annealing for 10 min (cooling), (3) unloading the force to preload value (0.01 N) at a rate of 0.05 N/min and annealing for 10 min (unloading and shape fixing), and (4) reheating the sample to 120 °C and annealing for 20 min (recovery). This 1W-SMC (steps 1−4) is conducted three more times on the same sample.

For 2W-SMCs, only temperature is varied from 60 to 120 °C, while the applied force is constant. The following procedure is used to characterize 2W-SME of XL-TP-*n*: (1) heating the sample to 120 °C and annealing for 30 min, (2) applying prescribed force to the sample at 120 °C, (3) cooling the sample to 60 °C at a rate of 3 °C/min and annealing for 20 min, and (4) reheating the sample to 120 °C at a rate of 3 °C/min and annealing for 20 min. Steps 3 and 4 are repeated three more times on the same sample.

Acknowledgment. The authors thank Prof. P. T. Mather (Syracuse University) and Dr. H. Qin (Lubrizol Corp.) for helpful discussions regarding determination of thermal transitions by DMA. The authors also thank J. Jang (Honda Motor Co.) for improving quality of illustrations in this publication. Financial support was provided by the University of Connecticut new-faculty start-up fund, University of Connecticut Research Foundation faculty grant, and NSF CAREER Award to R.M.K. (DMR-0748398). Central instrumentation facilities in the Institute of Materials Science and Chemistry Department are acknowledged.

Supporting Information Available: Polarized optical microscope (POM) images, 2D-WAXS, temperature-controlled SAXS, and entire T_{cl}-based 1W-SMCs. This material is available free of charge *via* the Internet at http://pubs.acs.org.

REFERENCES AND NOTES

1. El Feninat, F.; Laroche, G.; Fiset, M.; Mantovani, D. Shape Memory Materials for Biomedical Applications. *Adv. Eng. Mater.* **2002,** *4*, 91–104.
2. Small, I. V. W.; Singhal, P.; Wilson, T. S.; Maitland, D. J. Biomedical Applications of Thermally Activated Shape Memory Polymers. *J. Mater. Chem.* **2010,** *20*, 3356–3366.
3. Sokolowski, W.; Metcalfe, A.; Hayashi, S.; Yahia, L. H.; Raymond, J. Medical Applications of Shape Memory Polymers. *Biomed. Mater.* **2007,** *2*, S23–S27.
4. Yakacki, C. M.; Gall, K. Shape-Memory Polymers for Biomedical Applications. *Adv. Polym. Sci.* **2010,** *226*, 147–175.
5. Lendlein, A.; Langer, R. Biodegradable, Elastic Shape-Memory Polymers for Potential Biomedical Applications. *Science* **2002,** *296*, 1673–1676.
6. Chen, M. C.; Tsai, H. W.; Chang, Y.; Lai, W. Y.; Mi, F. L.; Liu, C. T.; Wong, H. S.; Sung, H. W. Rapidly Self-Expandable Polymeric Stents with a Shape-Memory Property. *Biomacromolecules* **2007,** *8*, 2774–2780.
7. Xue, L. A.; Dai, S. Y.; Li, Z. Biodegradable Shape-Memory Block Copolymers for Fast Self-Expandable Stents. *Biomaterials* **2010,** *31*, 8132–8140.
8. Thornton, A. J.; Alsberg, E.; Albertelli, M.; Mooney, D. J. Shape-Defining Scaffolds for Minimally Invasive Tissue Engineering. *Transplantation* **2004,** *77*, 1798–1803.
9. Migneco, F.; Huang, Y.-C.; Birla, R. K.; Hollister, S. J. Poly(glycerol-dodecanoate), a Biodegradable Polyester for Medical Devices and Tissue Engineering Scaffolds. *Biomaterials* **2009,** *30*, 6479–6484.
10. Neuss, S.; Blomenkamp, I.; Stainforth, R.; Boltersdorf, D.; Jansen, M.; Butz, N.; Perez-Bouza, A.; Knuechel, R. The Use of a Shape-Memory Poly(ε-caprolactone)dimethacrylate Network as a Tissue Engineering Scaffold. *Biomaterials* **2009,** *30*, 1697–1705.
11. Nagahama, K.; Ueda, Y.; Ouchi, T.; Ohya, Y. Biodegradable Shape-Memory Polymers Exhibiting Sharp Thermal Transitions and Controlled Drug Release. *Biomacromolecules* **2009,** *10*, 1789–1794.
12. Neffe, A. T.; Hanh, B. D.; Steuer, S.; Lendlein, A. Polymer Networks Combining Controlled Drug Release, Biodegradation, and Shape Memory Capability. *Adv. Mater.* **2009,** *21*, 3394–3398.
13. Wischke, C.; Neffe, A. T.; Steuer, S.; Lendlein, A. Evaluation of a Degradable Shape-Memory Polymer Network as Matrix for Controlled Drug Release. *J. Controlled Release* **2009,** *138*, 243–250.
14. Wischke, C.; Neffe, A. T.; Lendlein, A. Controlled Drug Release from Biodegradable Shape-Memory Polymers. *Adv. Polym. Sci.* **2010,** *226*, 177–205.
15. Behl, M.; Razzaq, M. Y.; Lendlein, A. Multifunctional Shape-Memory Polymers. *Adv. Mater.* **2010,** *22*, 3388–3410.
16. Kunzelman, J.; Chung, T.; Mather, P. T.; Weder, C. Shape Memory Polymers with Built-In Threshold Temperature Sensors. *J. Mater. Chem.* **2008,** *18*, 1082–1086.
17. DiOrio, A. M.; Luo, X.; Lee, K. M.; Mather, P. T. A Functionally Graded Shape Memory Polymer. *Soft Matter* **2011,** *7*, 68–74.
18. Burke, K. A.; Mather, P. T. Soft Shape Memory in Main-Chain Liquid Crystalline Elastomers. *J. Mater. Chem.* **2010,** *20*, 3449–3457.
19. Xie, T.; Xiao, X.; Li, J.; Wang, R. Encoding Localized Strain History through Wrinkle Based Structural Colors. *Adv. Mater.* **2010,** *22*, 4390–4394.
20. Wang, R.; Xie, T. Shape Memory and Hydrogen Bonding-Based Strong Reversible Adhesive System. *Langmuir* **2010,** *26*, 2999–3002.
21. Xie, T.; Xiao, X. Self-Peeling Reversible Dry Adhesive System. *Chem. Mater.* **2008,** *20*, 2866–2868.
22. Hu, J.; Chen, S. A Review of Actively Moving Polymers in Textile Applications. *J. Mater. Chem.* **2010,** *20*, 3346–3355.
23. Ohm, C.; Brehmer, M.; Zentel, R. Liquid Crystalline Elastomers as Actuators and Sensors. *Adv. Mater.* **2010,** *22*, 3366–3387.
24. Mirfakhrai, T.; Madden, J. D. W.; Baughman, R. H. Polymer Artificial Muscles. *Mater. Today* **2007,** *10*, 30–38.
25. Li, M.-H.; Keller, P. Artificial Muscles Based on Liquid Crystal Elastomers. *Philos. Trans. R. Soc. A* **2006,** *364*, 2763–2777.
26. Warner, M.; ; Terentjev, E. M. *Liquid Crystal Elastomers*; Oxford University Press: Oxford, UK, 2003.

27. Rousseau, I. A.; Mather, P. T. Shape Memory Effect Exhibited by Smectic-C Liquid Crystalline Elastomers. *J. Am. Chem. Soc.* **2003,** *125*, 15300–15301.
28. Qin, H.; Mather, P. T. Combined One-Way and Two-Way Shape Memory in a Glass-Forming Nematic Network. *Macromolecules* **2009,** *42*, 273–280.
29. Hiraoka, K.; Sagano, W.; Nose, T.; Finkelmann, H. Biaxial Shape Memory Effect Exhibited by Monodomain Chiral Smectic C Elastomers. *Macromolecules* **2005,** *38*, 7352–7357.
30. Hiraoka, K.; Tagawa, N.; Baba, K. Shape-Memory Effect Controlled by the Crosslinking Topology in Uniaxially-Deformed Smectic C* Elastomers. *Macromol. Chem. Phys.* **2008,** *3*, 298–307.
31. Ahir, S. V.; Tajbakhsh, A. R.; Terentjev, E. M. Self-Assembled Shape-Memory Fibers of Triblock Liquid-Crystal Polymers. *Adv. Funct. Mater.* **2006,** *16*, 556–560.
32. Ahn, S.-k.; Deshmukh, P.; Kasi, R. M. Shape Memory Behavior of Side-Chain Liquid Crystalline Polymer Networks Triggered by Dual Transition Temperatures. *Macromolecules* **2010,** *43*, 7330–7340.
33. Ahn, S.-k.; Nguyen Le, L. T.; Kasi, R. M. Synthesis and Characterization of Side-Chain Liquid Crystalline Polymers Bearing Cholesterol Mesogen. *J. Polym. Sci., Part A: Polym. Chem.* **2009,** *47*, 2690–2701.
34. Mano, J. F.; Gómez Ribelles, J. L. Mechanical Spectroscopy Studies on a Side-Chain Liquid Crystalline Polysiloxane. Comparison with Dielectric and DSC Data. *Macromolecules* **2003,** *36*, 2816–2824.
35. Craig, A. A.; Winchester, I.; Madden, P. C.; Larcey, P.; Hamley, I. W.; Imrie, C. T. Synthesis, Thermal Characterization and Rheological Properties of a Homologous Series of Polymethacrylate-Based Side-Chain Liquid Crystal Polymers. *Polymer* **1998,** *39*, 1197–1205.
36. Lee, K. M.; Han, C. D. Effect of Flexible Spacer Length on the Rheology of Side-Chain Liquid-Crystalline Polymers. *Macromolecules* **2003,** *36*, 8796–8810.
37. The distances of the SmA layer (d_1) for homopolymer of NBCh5, NBCh10, and NBCh15 are 53.0, 61.2 and 44.9 Å, respectively.
38. Percec, V.; Hahn, B.; Ebert, M.; Wendorff, J. H. Liquid-Crystalline Polymers Containing Heterocycloalkanediyl Groups as Mesogens. 8. Morphological Evidence for Microphase Separation in Poly(methylsiloxane-*co*-dimethylsiloxane)s Containing 2-[4-(2(S)-Methyl-1-butoxy)phenyl]-5-(11-undecanyl)-1,3,2-dioxaborinane Side Groups. *Macromolecules* **1990,** *23*, 2092–2095.
39. Sahlén, F.; Peterson, M. C.; Percec, V.; Hult, A.; Gedde, U. W. Smectic A Organisation in Copolymers of *i*-Butyl Vinyl Ether and 11-[(4′-Cyano-4-biphenyl)oxy]undecanyl Vinyl Ether As Assessed by X-ray Scattering. *Polym. Bull.* **1995,** *35*, 629–634.
40. Gopinadhan, M.; Beach, E. S.; Anastas, P. T.; Osuji, C. O. Smectic Demixing in the Phase Behavior and Self-Assembly of a Hydrogen-Bonded Polymer with Mesogenic Side Chains. *Macromolecules* **2010,** *43*, 6646–6654.
41. McArdle, C. B. *Side Chain Liquid Crystal Polymers*; Chapman and Hall: New York, 1989.
42. Nishikawa, E.; Finkelmann, H. Orientation Behavior of Smectic Polymer Networks by Uniaxial Mechanical Fields. *Macromol. Chem. Phys.* **1997,** *198*, 2531–2549.
43. Hardouin, F.; Achard, M. F.; Destrade, C.; Tinh, N. H. Unusual Bilayered Fluid Smectic Modifications in Polar Series. *J. Phys. (Paris)* **1984,** *45*, 765–769.
44. Imrie, C. T.; Schleeh, T.; Karasz, F. E.; Attard, G. S. Dependence of the Transitional Properties of Polystyrene-Based Side-Chain Liquid-Crystalline Polymers on the Chemical Nature of the Mesogenic Group. *Macromolecules* **1993,** *26*, 539–544.
45. Yamaguchi, T.; Asada, T. Coexistence of Two Different Side Chain Packing Structures in a Smectic Phase of Liquid-Crystalline Side Chain Polymers. *Liq. Cryst.* **1991,** *10*, 215–228.
46. Yamaguchi, T.; Asada, T.; Hayashi, H.; Nakamura, N. Dependence of the Packing Structure of Mesogenic Groups on the Flexible Spacer Length of Liquid-Crystalline Side-Chain Polymers. *Macromolecules* **1989,** *22*, 1141–1144.
47. Zhang, J. H.; Bazuin, C. G.; Freiberg, S.; Brisse, F.; Zhu, X. X. Effect of Side Chain Structure on the Liquid Crystalline Properties of Polymers Bearing Cholesterol, Dihydrocholesterol and Bile Acid Pendant Groups. *Polymer* **2005,** *46*, 7266–7272.
48. Liu, C.; Qin, H.; Mather, P. T. Review of Progress in Shape-Memory Polymers. *J. Mater. Chem.* **2007,** *17*, 1543–1558.
49. Lendlein, A.; Kelch, S. Shape-Memory Polymers. *Angew. Chem., Int. Ed.* **2002,** *41*, 2034–2057.
50. Chung, T.; Romo-Uribe, A.; Mather, P. T. Two-Way Reversible Shape Memory in a Semicrystalline Network. *Macromolecules* **2008,** *41*, 184–192.
51. Behl, M.; Bellin, I.; Kelch, S.; Wagermaier, W.; Lendlein, A. One-Step Process for Creating Triple-Shape Capability of AB Polymer Networks. *Adv. Funct. Mater.* **2009,** *19*, 102–108.
52. Bellin, I.; Kelch, S.; Lendlein, A. Dual-Shape Properties of Triple-Shape Polymer Networks with Crystallizable Network Segments and Grafted Side Chains. *J. Mater. Chem.* **2007,** *17*, 2885–2891.